Liquid Crystals
Publication details, including instructions for authors and subscription information:
http://www.informaworld.com/smpp/title~content=t713926090

X-ray diffraction analysis of the layer structure in a ferroelectric liquid crystal with a chiral nematic-chiral smectic C phase transition

Ray Hasegawa Corresponding author[a]; Aira Hotta[a]; Kohki Takatoh[a]
[a] Display Materials and Devices Laboratory, Corporate Research & Development Center, Komukai Toshiba-cho, Saiwai-ku, Kawasaki 212-8582, Japan

Online publication date: 12 May 2010

To cite this Article Hasegawa Corresponding author, Ray , Hotta, Aira and Takatoh, Kohki(2004) 'X-ray diffraction analysis of the layer structure in a ferroelectric liquid crystal with a chiral nematic-chiral smectic C phase transition', Liquid Crystals, 31: 3, 431 — 442
To link to this Article: DOI: 10.1080/02678290410001666039
URL: http://dx.doi.org/10.1080/02678290410001666039

LIQUID CRYSTALS, VOL. 31, NO. 3, MARCH 2004, 431–442

Taylor & Francis
Taylor & Francis Group

X-ray diffraction analysis of the layer structure in a ferroelectric liquid crystal with a chiral nematic–chiral smectic C phase transition

RAY HASEGAWA*, AIRA HOTTA and KOHKI TAKATOH

Display Materials and Devices Laboratory, Corporate Research & Development Center, Toshiba Corporation, 1, Komukai Toshiba-cho, Saiwai-ku, Kawasaki 212-8582, Japan

(*Received 14 July 2003; in final form 1 December 2003; accepted 1 December 2003*)

A half-V-shaped switching ferroelectric liquid crystal (FLC) is a promising candidate for fast response displays. In the half-V FLC display, a liquid crystal with a chiral nematic–chiral smectic C phase transition is used, and the smectic layer is formed by cooling from N* to SmC* with an applied d.c. field. We studied the layer structure by means of X-ray measurements for two axes (ω and χ). By using a point-focused X-ray tube and optimizing the slit width, we succeeded in the two-axis measurement with a commercial X-ray system. The ω–χ profile of the half-V FLC showed two broad peaks in an arc-shaped high-intensity area. Our interpretation of this result is that the major part of the layer consists of a tilted-bookshelf structure and that the minor part consists of a near-bookshelf structure. Since optical microscopy observations on the half-V FLC cells showed a stripe-shaped texture, we consider that the coexistence of the tilted-bookshelf and the near-bookshelf structures forms the stripe-shaped patterns. The radius of the arc-shaped high-intensity area was nearly equal to the molecular tilt angle. This result can explain why the half-V FLC showed a desirable black appearance in spite of the stripe-shaped texture.

1. Introduction

A twisted nematic (TN) liquid crystal display (LCD) combined with an array of thin film transistors (TFTs), i.e. a TN-mode TFT-LCD, is widely used for cellular phones, personal computers, TVs, etc. However, for applications to high-definition TVs and the display of high-quality moving pictures from digital sources, the response speed of the TN-mode is insufficient. Since the response speeds of a ferroelectric liquid crystal (FLC) and an antiferroelectric liquid crystal (AFLC) are much faster than that of the TN-mode, various TFT-LCDs using FLC and AFLC materials have been developed [1]. The present authors have demonstrated a 15-inch TFT-LCD with XGA resolution using a V-shaped switching smectic liquid crystal (thresholdless AFLC) [2, 3].

Several groups have developed a half-V-shaped switching ferroelectric liquid crystal (half-V FLC) display [4, 5]. The half-V FLC mode is a promising candidate for a fast response TFT-LCD because it has low spontaneous polarization ($\mathbf{P}_s$) and allows the display of analogue grey scale. Moreover, it provides a non-hold type display [6, 7] by simple a.c. driving. In the half-V FLC display, a liquid crystal with a chiral nematic–chiral smectic C (N*–SmC*) phase transition is used and the smectic layer is formed by cooling from N* to SmC* under an applied d.c. electric field. In many cases, the texture of the half-V FLC consists of unclear striped domains parallel to the rubbing direction. In order to obtain a defect-free and stable alignment of the liquid crystal, an adequate understanding of the layer structure is necessary.

In order to investigate the layer structures in smectic liquid crystals, X-ray diffraction (XRD) is widely used. The X-ray measurement for the ω-axis provides information about the layer tilt in the direction vertical to the substrate plane of a cell, and that for the χ-axis provides information about the layer rotation in the direction horizontal to the substrate plane. In the case of an FLC with a smectic A (SmA) to SmC* phase transition, in general the layer normal is fixed approximately parallel to the rubbing direction and the layer rotation angle is about 0°. Thus, the layer structure is generally analysed by XRD for only the ω-axis.

*Author for correspondence;
e-mail: ray.hasegawa@toshiba.co.jp

Liquid Crystals ISSN 0267-8292 print/ISSN 1366-5855 online © 2004 Taylor & Francis Ltd
http://www.tandf.co.uk/journals
DOI: 10.1080/02678290410001666039

In contrast, in the case of an FLC with a N*–SmC* phase transition, and thus having no SmA phase, on cooling the liquid crystal from the N* phase with no applied d.c. electric field two types of domain with the $\mathbf{P}_s$ directing upwards or downwards are formed [8–12]. Consequently, the layer normals in these domains are not fixed in one direction. In the case of the half-V FLC mode, one type of domain with the $\mathbf{P}_s$ directing either upwards or downwards can be selectively formed by applying a d.c. electric field during the N*–SmC* phase transition. However, the stripe-shaped texture observed in the half-V FLC cells implies a distribution of the layer rotation angle. Thus, in order to investigate the layer structures in an FLC with an N*–SmC* phase transition, including the half-V FLC, X-ray measurement for not only the ω-axis but also the χ-axis is required.

Almost all the X-ray measurements for the two axes (ω and χ) have been carried out using synchrotron X-rays [13–20]. Takada *et al.* [13] investigated the layer structure of an FLC with an N*–SmC* phase transition at the Photon Factory in Tsukuba, Japan. Although the synchrotron is a powerful tool for the analysis of various liquid crystals [21–23], a special experimental facility is needed. So we attempted the two-axis measurement using a commercially produced X-ray diffractometer. By the use of a point-focused X-ray tube and optimization of the slit width, the divergence of the X-ray beam was reduced and consequently the two-axis measurement was achieved.

In this study, the layer structures in an FLC with an N*–SmC* phase transition, including the half-V FLC, were analysed with the commercial X-ray system. In addition, relationships between the layer structures and the liquid crystal alignment were investigated.

2. Experimental

In our two-axis X-ray measurements (ω–χ profiles), a Philips (PANalytical) X'pert-MRD X-ray diffractometer equipped with a point-focused X-ray tube with a Cu target anode was used. The X-ray beam was not monochromatized and the main component of the beam was a CuK_α line (0.1542 nm). The width of the incident and diffracted beam slit was optimized to reduce the divergence of the X-ray beam (see § 3.2). The incident beam size in a typical experiment was about 0.6 mm (vertical) × 3 mm (horizontal) at the sample position. All the two-axis measurements were carried out at room temperature, the step of the sample rotation was 1°, and the data collection time of each step was 2.5 s.

The diffraction geometry is schematically shown in figure 1. The X-ray detector (proportional counter) was fixed at the $2\theta_B$ corresponding to the smectic layer spacing, where θ_B is the Bragg angle. The ω-scan is the sample rotation around the same axis as the $2\theta_B$ rotation. The ω-scan profile provides the layer tilt angle δ in the direction vertical to the substrate plane. The χ-scan is the sample rotation perpendicular to the ω-rotation, and the direction of χ-axis is parallel to the substrate normal. In the case that the rubbing direction of the sample is parallel to the $2\theta_B$ rotation plane, χ is defined as 0°. The χ-scan profile provides the layer rotation angle α in the direction horizontal to the substrate plane.

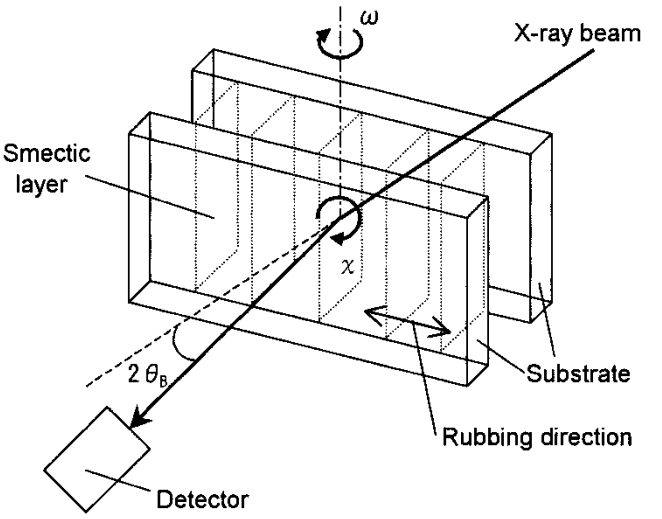

Figure 1. The diffraction geometry in the two-axis X-ray measurements.

Figure 2 summarizes the relationships between the layer structures and the ω–χ profiles with the peak at (a) $\omega = \chi = 0°$, (b) $\omega = \delta$, $\chi = 0°$ and (c) $\omega = 0°$, $\chi = \alpha$. The layer structures of figures 2 (*a*) and 2 (*b*) are bookshelf and tilted-bookshelf, respectively. Although the structure of figure 2 (*c*) is so-called bookshelf in the direction vertical to the substrate plane, the layer normal rotates at the angle of α from the rubbing direction.

In order to obtain high transparency of the X-ray beam, an 80 μm thick glass substrate with an indium tin oxide (ITO) electrode was used. The half-V FLC materials (LZ-4008 and LZ-4011, supplied by Clariant Japan K. K., see table 1) were injected at 95°C between a pair of the substrates with a gap of approximately 1.5 μm. On both of the inner surfaces of the substrates, polyimide (SE-7992, Nissan Chemical Industries, Ltd) films with low pretilt angle were formed and rubbed in the conventional manner to obtain alignment layers whose thickness was about 45 nm. The FLC materials LZ-4008 and LZ-4011 consisted of similar components with a phenylpyrimidine core; however, the molecular

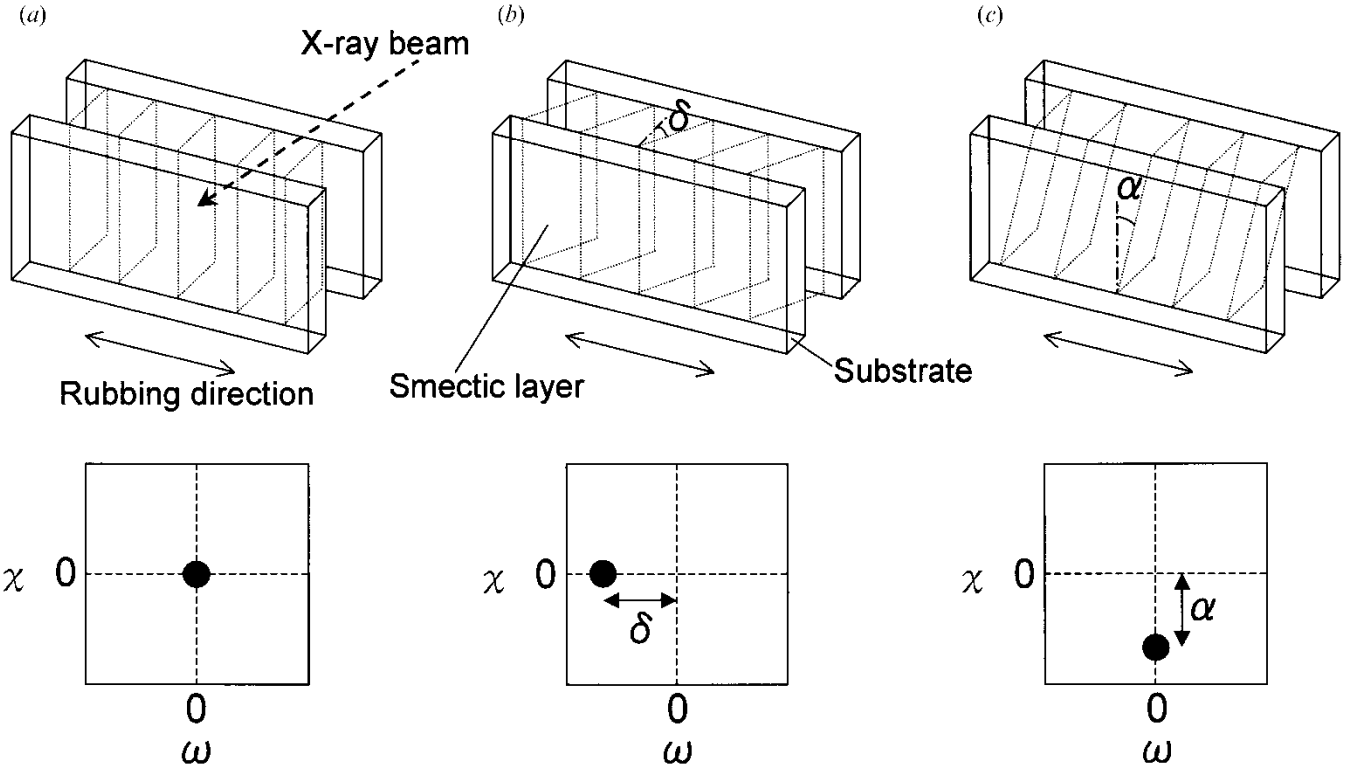

Figure 2. Schematic ω–χ profiles in the two-axis X-ray measurements for typical layer structures; (*a*) bookshelf, (*b*) tilted-bookshelf, (*c*) vertical bookshelf with the layer normal rotated at an angle α from the rubbing direction.

Table 1. Properties of the liquid crystal materials.

LZ-4008:						
Phase sequence crystal	$<0°C$	SmC*	61°C	N*	88°C	Isotropic
Spontaneous polarization ($\mathbf{P}_s$)				2.7 nC cm^{-2}		
Tilt angle at room temperature				21.1°		
LZ-4011:						
Phase sequence crystal	$<0°C$	SmC*	63°C	N*	86°C	Isotropic
Spontaneous polarization ($\mathbf{P}_s$)				2.9 nC cm^{-2}		
Tilt angle at room temperature				27.3°		

tilt angles and the N*–SmC* phase transition properties of these materials were different.

We evaluated four samples, as listed in table 2. Rubbing treatment in the direction antiparallel (1, 2, 4) or parallel (3) was performed on a pair of the polyimide films (cf. figures 9, 13 and 15). Samples 1–3 were cooled from the N* to SmC* phase with an applied d.c. voltage of -5 V. Sample 4 was cooled from N* to SmC* with no applied d.c. field.

Table 2. List of the sample cells.

Sample	Materials	Rubbing	Cooling	Texture
1[a]	LZ-4008	Antiparallel	With d.c.	Striped domain
2[a]	LZ-4011	Antiparallel	With d.c.	Striped domain
3	LZ-4008	Parallel	With d.c.	Monodomain
4	LZ-4008	Antiparallel	Without d.c.	APD

[a]Samples 1 and 2 showed a common half-V switching.

For the measurements of transmittance–applied voltage (T–V) dependence and tilt angle, a polarizing optical microscope (BX50, Olympus Optical Co.) with a photodiode was used. The cone angle (i.e. the double of the molecular tilt angle θ_{tilt}) was determined from the extinction positions of the sample when $+10$ V and -10 V were applied. The order of phase transition of the FLC materials was evaluated by differential scanning calorimetry (DSC). The DSC measurements were carried out at a rate of 10°C min^{-1} by using a DSC220CU instrument (Seiko Instruments Inc.); the sample weight was about 6 mg.

3. Results and discussion

3.1. *Texture and electro-optical properties*

The optical properties of the sample cells are presented here before the results of X-ray analysis. Figure 3 shows micrographs of samples 1, 3 and 4 in the absence of an electric field, which were taken using a polarizing optical microscope at room temperature. The transmission axis of one polarizer was placed nearly parallel to the rubbing direction, and the transmission axis of the other was placed perpendicular to it.

Samples 1 and 2 had stripe-shaped texture, with the stripes running almost parallel to the rubbing direction (see figure 3 (*a*)). The size of each domain was much smaller than the pixel size of ordinary LCDs. Light leakage from the domains and the domain boundaries was low. This type of texture is commonly observed in half-V cells. *T–V* dependence was measured for a test cell made with a pair of 1.1 mm thick glass substrates under the same conditions as for sample 2. As shown in figure 4, half-V shaped switching was obtained, i.e. the transmittance was almost constant at negative polarity of the applied voltage, and increased with a higher voltage at positive polarity. The dependence exhibited a slight hysteresis.

As shown in figure 3 (*b*), monodomain texture was observed in sample 3. Parallel rubbing was performed for sample 3, which may affect the generation of the monodomain texture. The hysteresis loop of sample 3 in *T–V* dependence was so large that the sample was unsuitable for the display of grey scale.

Sample 4 was prepared by cooling from N* to SmC* with no applied d.c. electric field. Consequently, two types of domain were formed, which can be seen as grey and black stripes in figure 3 (*c*). These corresponded to 'up' and 'down' states of the $\mathbf{P}_s$ and are named alternating polarization domains (APDs) [12]. The directions of molecular alignment in the two types of domain differed by several degrees; the domain stripes ran parallel to the rubbing direction. Obvious light leakage was observed from some parts of the domain boundaries. Note that the size of the X-ray analysing area was much larger than that of each domain.

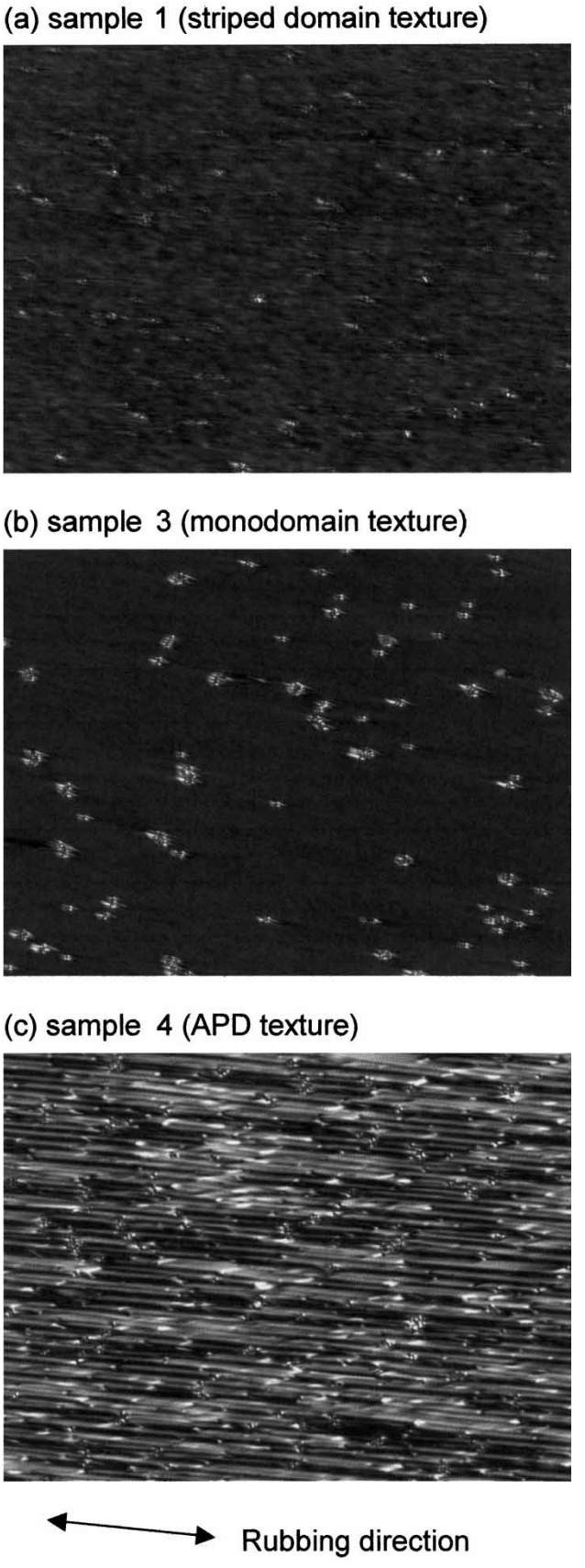

Figure 3. Micrographs of samples 1, 3 and 4 in the absence of an electric field, taken using a polarizing optical microscope (crossed nicols). The size of the micrographs is 225 μm (vertical) × 300 μm (horizontal). White dots in the micrographs were caused by the spacers for cell gap control and inhomogeneous alignment of the liquid crystal around the spaces. The texture of sample 2 was similar to that of sample 1.

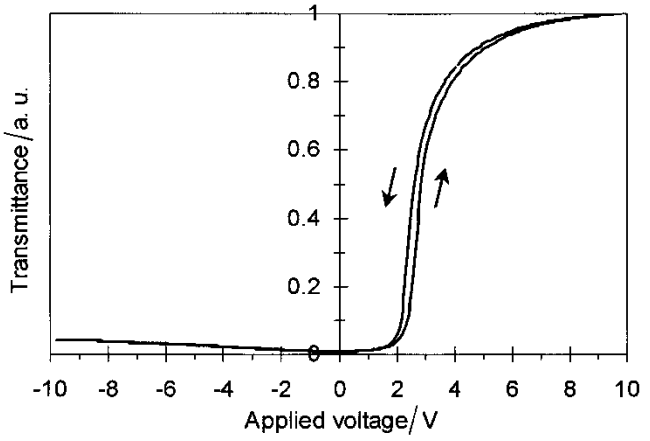

Figure 4. Transmittance–applied voltage dependence of a test cell made with a pair of 1.1 mm thick glass substrates under the same conditions as for sample 2. The dependence was measured at room temperature by applying a triangular wave voltage at a frequency of 0.1 Hz.

3.2. *Experimental improvement of the X-ray diffractometer*

In the case of one axis (ω-axis) measurement, divergence of the X-ray beam in a vertical direction (perpendicular to the $2\theta_B$ rotation plane) has hardly any effect on the experimental result. Thus, a line-focused X-ray tube and a detector with rectangular (length greater than width) window are often used. In contrast, in the case of the two-axis measurement, such a set-up caused an inaccurate χ-profile. The set-up for the two-axis measurement is schematically shown in figure 5. In order to reduce the divergence of the X-ray beam in a vertical direction, an incident beam slit (cross slit collimator) was placed between the X-ray tube and the sample. Additionally, a diffracted beam slit was inserted in front of the detector to narrow its rectangular window.

The χ-profiles (rocking curve) of sample 2 were measured under various conditions while the ω-angle was set to the peak position ($\omega = -17.9°$). The influence of the slit-width and the X-ray tube arrangement (point- or line-focus) on the χ-profiles is shown in figure 6. In the case of the line-focused X-ray tube, (a) and (b), no clear peak was observed, even if the slit width had narrowed. Thus, for the two-axis measurement, it was necessary to change the arrangement of the X-ray tube from line-focus to point-focus.

As shown in (c), by using the point-focused X-ray tube and optimizing the slit-width, a relatively sharp peak with acceptable signal-to-noise ratio was obtained. Although the wider incident and diffracted beam slits enhanced the X-ray intensity, the obtained peak was broad and the peak position shifted toward 0°, see (d) and (e). These results indicate that the peak position, i.e. the layer rotation angle, cannot be determined accurately by measurement with the wider slit. The two-axis X-ray measurements reported in the following sections were performed at the optimized condition shown in (c) of figure 6.

3.3. *ω–χ profiles of the half-V FLC cells (samples 1 and 2)*

The ω–χ profiles of samples 1 and 2 were measured (see figures 7 and 8, respectively). These samples were

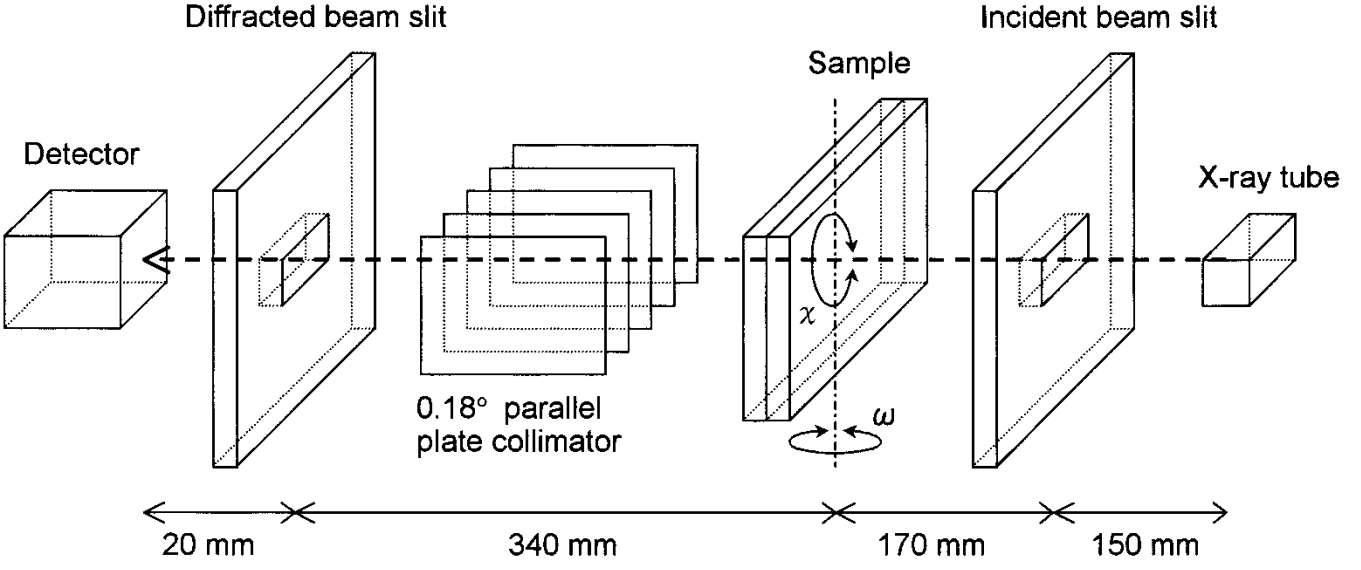

Figure 5. The experimental set-up for the two-axis X-ray measurement. An incident beam slit was used to reduce the divergence of the X-ray beam; a diffracted beam slit narrowed the detector window.

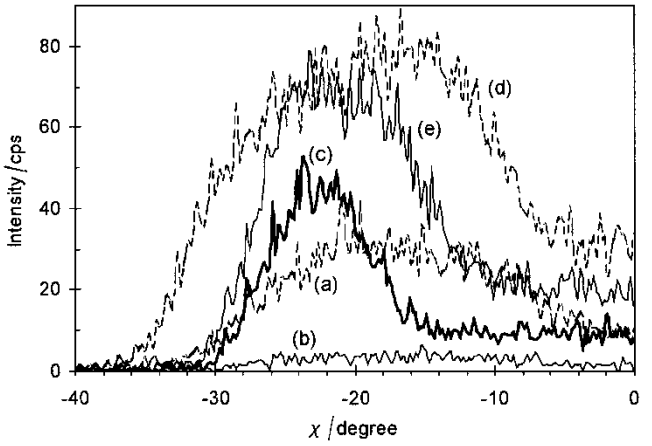

Profile	Focus	Incident beam slit	Diffracted beam slit
		vertical horizontal	vertical horizontal
(a)	line	2.0 x 2.0 mm	5.0 x 10 mm
(b)	line	0.5 x 2.0 mm	2.0 x 10 mm
(c)	point	0.5 x 2.0 mm	2.0 x 10 mm
(d)	point	2.0 x 2.0 mm	2.0 x 10 mm
(e)	point	0.5 x 2.0 mm	5.0 x 10 mm

Figure 6. The influence of the X-ray tube arrangement and slit-width on the χ-profiles (rocking curves) of sample 2, which were measured at a fixed ω-angle of -17.9°. Curve (c) illustrates the best condition, and the two-axis measurements were performed at this condition.

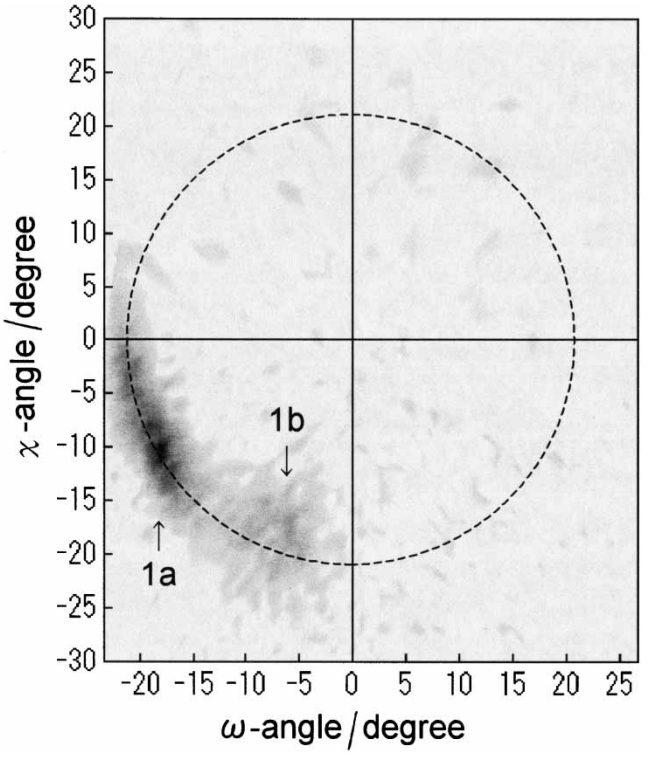

Figure 7. The ω–χ profile of sample 1 with stripe-shaped texture, measured at a fixed $2\theta_B$ angle of 3.41°. The dotted curve represents a circle with radius 21.0°. The darkest part corresponds to the highest diffracted intensity (54 cps).

prepared by cooling from N* to SmC* with an applied d.c. electric field and showed half-V switching. Both samples exhibited an arc-shaped high-intensity area. As shown in figure 7, sample 1 had two broad peaks in the high-intensity area. The centre position of the stronger peak (1a) was $\omega = -18^\circ$ and $\chi = -10^\circ$. This result indicates that the major part of sample 1 consists of a layer with $\delta \approx 18^\circ$ and $\alpha \approx 10^\circ$. The centre position of the weaker peak (1b) was $\omega = -6^\circ$ and $\chi = -17^\circ$. The circular dotted curve with a radius of 21.0° is drawn for eye-guide, and the arc-shaped high-intensity area was coincident with the curve in the region of $\omega \leqslant 0^\circ$ and $\chi \leqslant 0^\circ$.

As shown in figure 8, sample 2 also had two broad peaks in the arc-shaped high-intensity area. The centre position of the stronger peak (2a) was $\omega = -18^\circ$ and $\chi = -21^\circ$; that of the weaker peak (2b) was $\omega = -3^\circ$, $\chi = -27^\circ$. The radius of the high-intensity area was approximately 27.5°, which was larger than that of sample 1. Molecular tilt angles (measured using the polarizing microscope) of samples 1 and 2 were 21.1° and 27.3°, respectively. That is, the radii of the

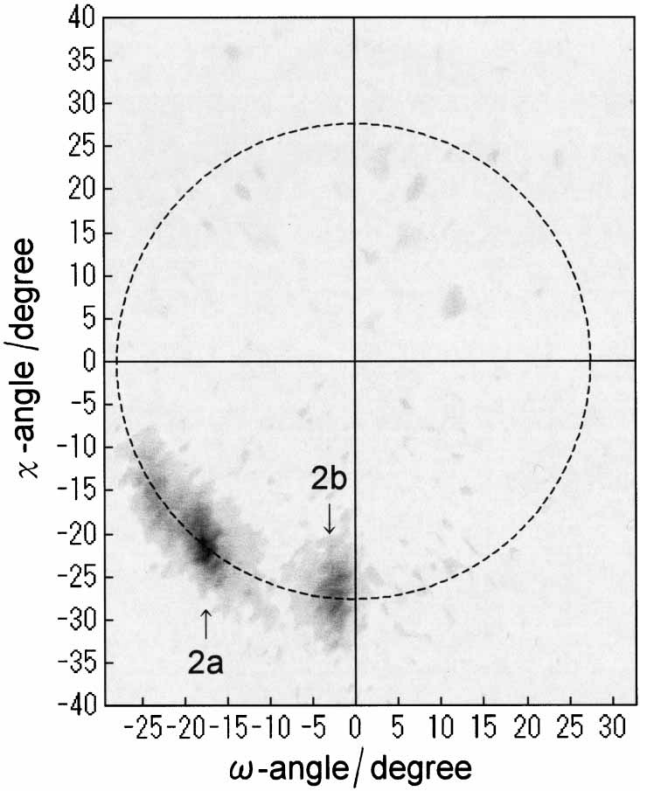

Figure 8. The ω–χ profile of sample 2 with stripe-shaped texture, measured at a fixed $2\theta_B$ angle of 3.46°. The dotted curve represents a circle with radius 27.5°. The darkest part corresponds to the highest diffracted intensity (56 cps).

high-intensity area were nearly equal to the molecular tilt angles.

3.4. *Proposed layer structure in the half-V FLC*

A layer structure in the half-V FLC is proposed on the basis of the results of the two-axis X-ray measurement and the optical microscopy observation, which is shown in figure 9. In the ω–χ profiles of the half-V FLC cells, two broad peaks in the arc-shaped high-intensity area were observed (see figures 7 and 8). The stronger peak (1a, 2a) has a relatively large absolute value of ω, indicating that the major part of the layer is a tilted-bookshelf structure in the vertical direction of the substrate plane. On the other hand, the ω-value of the weaker peak (1b, 2b) is close to 0°, indicating that the minor part of the layer is a near-bookshelf structure. Since the optical microscopy observations for the half-V FLC cells showed stripe-shaped texture, it is proposed that the co-existence of the two structures forms the stripe-shaped patterns. That is, the tilted-bookshelf structure observed as the stronger peak forms one kind of stripe and the near-bookshelf structure observed as the weaker peak forms another kind, illustrated as 'domain A' and 'domain B' in figure 9, respectively.

The absolute value of χ of the weaker peak is larger than that of the stronger peak and neither is close to 0°. This implies that the layer normals in both the domains A and B rotate from the rubbing direction and that the layer rotation angle α of domain B (the near-bookshelf structure) is larger than that of domain A (the tilted-bookshelf structure). Actually, the peaks obtained in the ω–χ profiles of the half-V FLC were broad compared with an ordinary FLC with an SmA–SmC* phase transition. This suggests that the distributions of the tilt angle and the rotation angle of the layer in the half-V FLC are relatively wide.

3.5. *Rationale for the layer in the half-V FLC*

In spite of the coexistence of the tilted-bookshelf structure and the near-bookshelf structure, the half-V FLC showed a desirable black appearance, resulting from the substantially coincident extinction position of each domain. In order to consider the reason, the position of the molecular director in the inclined smectic layer was calculated on the basis of reference [24].

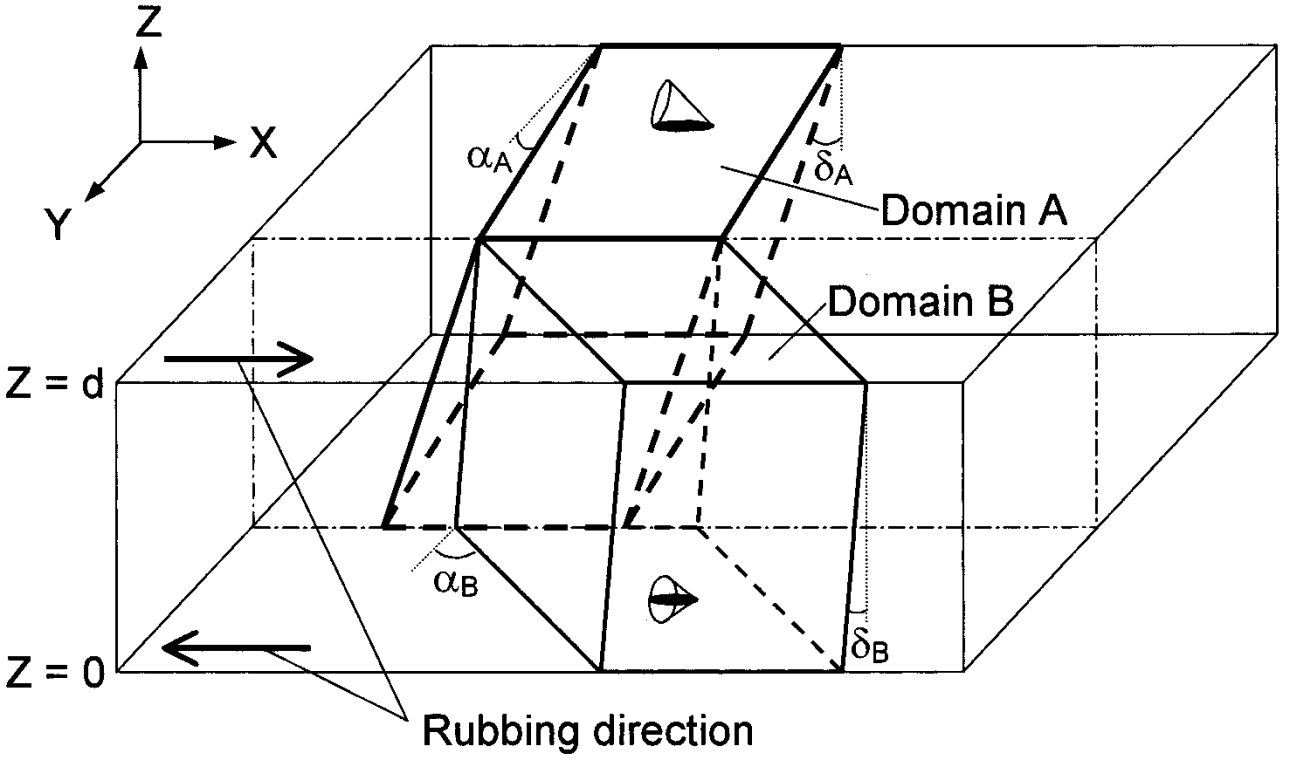

Figure 9. Schematic drawing of the proposed layer structure in the half-V FLC, possessing the stripe-shaped texture. The cell substrates lie in the XY-plane at the positions $Z=0$ and $Z=d$, where d is the cell gap. The rubbing direction is parallel to the X-axis; the angles are not drawn to scale. Domain A is a tilted-bookshelf structure with δ_A and α_A; domain B is a near-bookshelf structure with δ_B and α_B. The results of ω–χ profiles imply that the width of domain A is larger than that of domain B, and that $\delta_A > \delta_B$ and $\alpha_A < \alpha_B$.

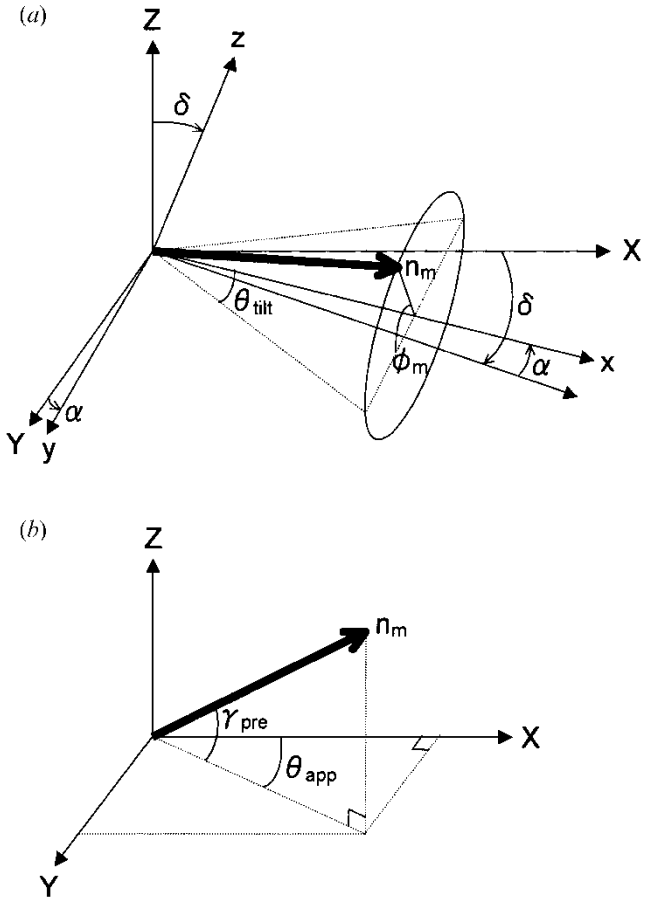

Figure 10. (*a*) Geometrical configuration of the FLC molecule (x, y, z); (*b*) laboratory (X, Y, Z) coordinates. The cell substrates lie in the XY-plane. The rubbing direction is parallel to the X-axis.

The coordinate systems of the liquid crystal (x, y, z) and the laboratory frame (X, Y, Z) are shown in figure 10. The liquid crystal molecular director $\mathbf{n}_m$ is given by

$$\mathbf{n}_m = (n_x, n_y, n_z) = (\cos\theta_{tilt},\ \sin\theta_{tilt}\ \cos\phi_m,\ \sin\theta_{tilt}\ \sin\theta_m) \quad (1)$$

where, θ_{tilt} and ϕ_m are the molecular tilt angle and the azimuthal rotation angle of a liquid crystal molecule, respectively.

The smectic layer is tilted from the substrate normal Z by δ. In addition, the layer normal is rotated from the rubbing direction X by α. The coordinate systems of the laboratory frame (X, Y, Z) is converted by

$$n_X = n_x\cos\delta\cos\alpha + n_z\sin\delta\cos\alpha + n_y\sin\alpha \quad (2)$$

$$n_Y = n_y\cos\alpha - n_x\cos\delta\sin\alpha - n_z\sin\delta\sin\alpha \quad (3)$$

$$n_Z = n_z\cos\delta - n_x\sin\delta. \quad (4)$$

From equations (1)–(4), the apparent tilt angle θ_{app} and the pretilt angle γ_{pre} of the FLC molecule are given by

$$\tan\theta_{app} = \frac{n_Y}{n_X} = \frac{(\sin\theta_{tilt}\cos\phi_m\cos\alpha - \cos\theta_{tilt}\cos\delta\sin\alpha - \sin\theta_{tilt}\sin\phi_m\sin\delta\sin\alpha)}{(\cos\theta_{tilt}\cos\delta\cos\alpha + \sin\theta_{tilt}\sin\phi_m\sin\delta\cos\alpha + \sin\theta_{tilt}\cos\phi_m\sin\alpha)} \quad (5)$$

$$\sin\gamma_{pre} = n_Z = \sin\theta_{tilt}\sin\phi_m\cos\delta - \cos\theta_{tilt}\sin\delta. \quad (6)$$

That is, in the layer with tilt angle δ and rotation angle α, the position of the molecular director (θ_{app} and γ_{pre}) is represented by using equations (5) and (6).

Polyimide alignment layers with low pretilt angle were used in this study. This suggests that the FLC molecules aligned approximately parallel to the substrate plane in the absence of the electric field. So we assume

$$\gamma_{pre} \approx 0^\circ. \quad (7)$$

In addition, the condition to make the FLC molecules align parallel to the rubbing direction is

$$\theta_{app} = 0^\circ. \quad (8)$$

By substitution of these values, equations (5) and (6) are described as the approximation expression

$$\theta_{tilt}^2 = \delta^2 + \alpha^2 = \omega^2 + \chi^2 \quad (9)$$

where $\delta = \omega$ and $\alpha = \chi$ at peak position in the ω–χ profiles. When equation (9) is satisfied, the molecular director aligns parallel to the rubbing direction with a pretilt angle of 0°.

As shown in figures 7 and 8, the high-intensity area was coincident with the circle of radius θ_{tilt}. That is, the smectic layer in the half-V FLC obeyed equation (9). As a result, the half-V FLC molecules aligned approximately parallel to the rubbing direction and a good black appearance was obtained in the half-V FLC cell.

In order to discuss the process of smectic layer formation at the N*–SmC* phase transition, DSC profiles of LZ-4008 and LZ-4011 were measured (figure 11). Peaks in enthalpy change at the N*–SmC* point were observed in both samples, indicating a first-order phase transition. In the case of a first-order transition, the smectic layer is formed directly at the N*–SmC* point; the liquid crystal molecules align parallel to the rubbing direction in the N* phase. The alignment can be maintained through the N*–SmC* phase transition when the layer inclines in the vertical and horizontal directions to the substrate plane, keeping the relation given by equation (9).

Compared with LZ-4011, the enthalpy changes of LZ-4008 at the N*–SmC* point were quite small (see figure 11). Note that the peak area of LZ-4008 at the isotropic–N* point was nearly equal to that of LZ-4011. The difference in the enthalpy change at the N*–SmC*

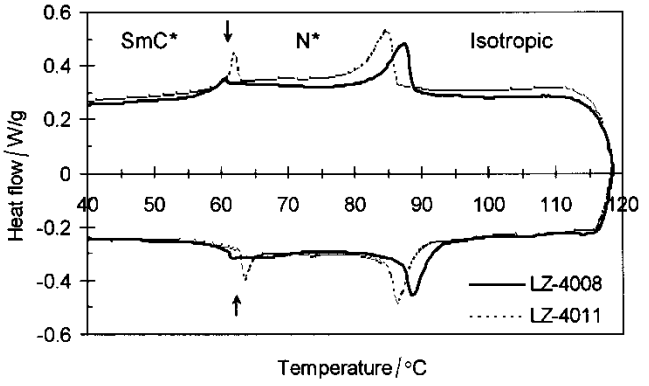

Figure 11. DSC profiles of LZ-4008 (solid line) and LZ-4011 (dotted line) measured on heating and cooling. Peaks in enthalpy change at the N*–SmC* point (indicated by arrows) were observed in both samples, indicating a first-order phase transition.

point may affect the formation of the smectic layer. For further investigation, X-ray measurements at a temperature near to the N*–SmC* point are necessary.

3.6. *ω–χ profile of the monodomain cell (sample 3)*

The ω–χ profile of sample 3 with monodomain texture was measured. As shown in figure 12, three peaks, a strong peak (3a: $\omega=-18^\circ$, $\chi=-12^\circ$), a weak peak (3b: $\omega=-5^\circ$, $\chi=-19^\circ$) and a medium peak (3c: $\omega=13^\circ$, $\chi=-15^\circ$), were observed. Since sample 3 consists of a single domain, the three peaks seem to originate from a single structure. The proposed layer structure is schematically shown in figure 13. The χ-values of 3a and 3c were roughly the same; the peak 3b is sufficiently weak to be neglected. Thus, these results imply that sample 3 has an asymmetric chevron structure inclined at angles of -18° and 13° to the direction vertical to the substrate plane, and that the layer normal rotates at an angle of 12°–15° from the rubbing direction.

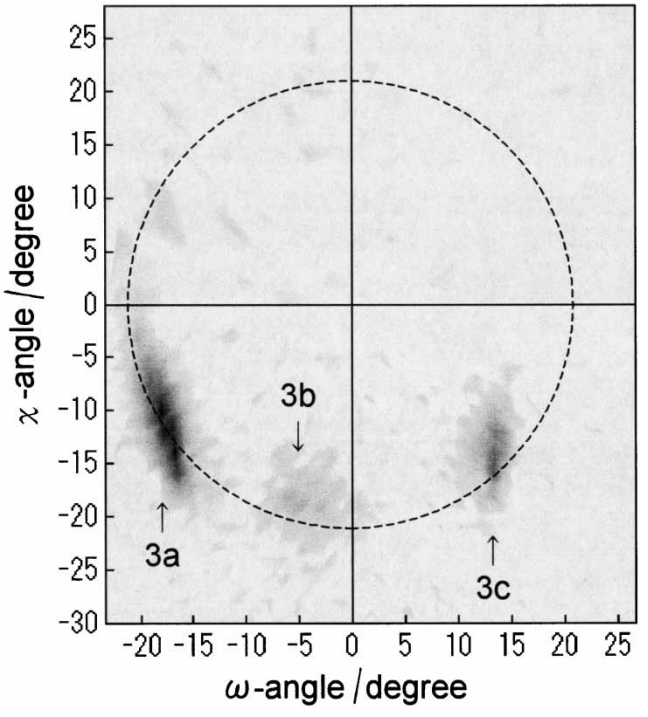

Figure 12. The ω–χ profile of sample 3 with monodomain texture, measured at a fixed $2\theta_B$ angle of 3.46°. The dotted curve represents a circle with radius 21.0°. The darkest part corresponds to the highest diffracted intensity (62 cps).

A comparison with sample 1 may be described as follows. Samples 1 and 3 were fabricated under the same conditions except for the rubbing direction. The peak positions of 3a and 3b were close to those of 1a and 1b, respectively (see figures 7 and 12). The peak intensity of 3b was much weaker than that of 1b, and another peak (3c) appeared in the region of $\omega>0^\circ$. Sample 1 with anti-parallel rubbing had a tilted-bookshelf-like structure and sample 3 with parallel rubbing had a chevron-like structure. This result can be explained by taking into account the pretilt angle of the FLC molecules on the surface of the rubbed polyimide films. Assuming that the layer inclined at the same direction for the pretilt of each surface, anti-parallel rubbing brings about the tilted-bookshelf structure and parallel rubbing brings about the chevron structure. Thus, sample 3 with parallel rubbing should have the chevron structure.

3.7. *ω–χ profile of the APD cell (sample 4)*

In figure 14, the ω–χ profile of sample 4 with APD texture shows the semicircular high-intensity area symmetrical with respect to the ω-axis. Since the major part of the high-intensity area is located around $\omega=-20^\circ$, the dominant structure in sample 4 is a tilted-bookshelf with $\delta\approx20^\circ$ in a direction vertical to the substrate plane. The direction of the layer normal is mainly distributed at a range of $\chi=\pm15^\circ$ from the rubbing direction. This result suggests a bent chevron structure in a direction horizontal to the substrate plane as illustrated in figure 15. Although some reports imply that the layer structure of an FLC with APDs is bookshelf in a direction vertical to the substrate plane (i.e. $\delta=0^\circ$), sample 4 showed a relatively high δ-value of around 20°. Compared with samples 1 and 2, the gap between the circle with radius 21.0° and the arc-shaped high-intensity area of sample 4 was relatively large, especially at the higher χ-value. This might cause the disagreement regarding extinction position in the APDs (see figure 3 (*c*)).

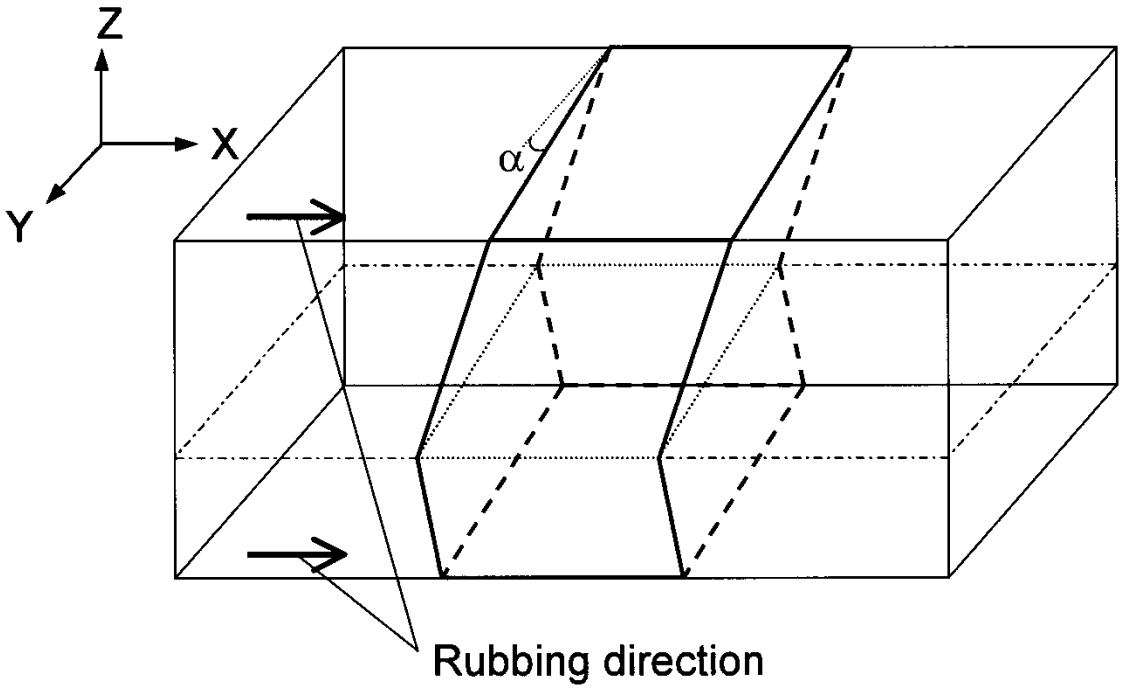

Figure 13. Schematic drawing of the proposed layer structure in sample 3, possessing the monodomain texture. The cell substrates lie in the XY-plane; the layer rotation angle α ranged between 12° and 15°.

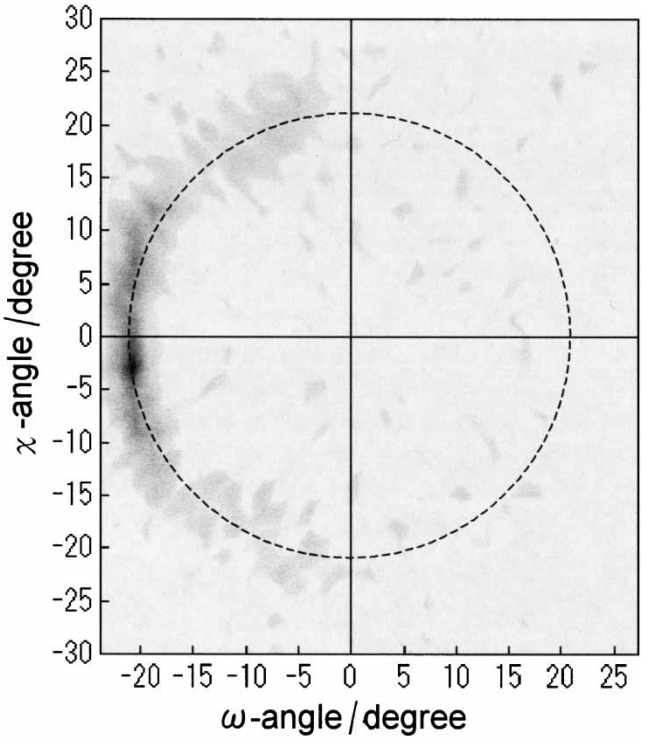

Figure 14. The ω–χ profile of sample 4 with APD texture, measured at a fixed $2\theta_B$ angle of 3.51°. The dotted curve represents a circle with radius 21.0°. The darkest part corresponds to the highest diffracted intensity (47 cps).

The difference between samples 1 and 4 depends on whether the smectic layer is formed with or without an applied d.c. electric field. The radii of the high-intensity areas of samples 1 and 4 are approximately 21°. The appearance of the high-intensity area of sample 4 was similar to that of the folded and piled up high-intensity area of sample 1 with respect to the line of $\chi = 0°$. Sample 4 was prepared by cooling from N* to SmC* with no applied d.c. electric field, and possessed two types of domain with 'up' and 'down' $\mathbf{P}_s$ states, illustrated as 'domain C' and 'domain D' in figure 15, respectively. Each type of domain corresponds to the high-intensity area in the region of either $\chi \leqslant 0°$ or $\chi \geqslant 0°$. On the other hand, in sample 1, one type of domain (either 'up' or 'down' $\mathbf{P}_s$ states) was selectively formed on application of a d.c. electric field during the N*–SmC* transition. Thus, the peaks of sample 1 were observed only in the region of $\chi \leqslant 0°$.

4. Conclusions

Two-axis X-ray measurements (ω–χ profiles) clarify the layer structure in the FLC with an N*–SmC* phase transition. The ω–χ profiles of the half-V FLC cells showed two broad peaks in an arc-shaped high-intensity area. Our interpretation of this result is that the major part of the layer consists of a tilted-bookshelf structure, the minor part consisting of a near-bookshelf structure. Since optical microscopy observations for the

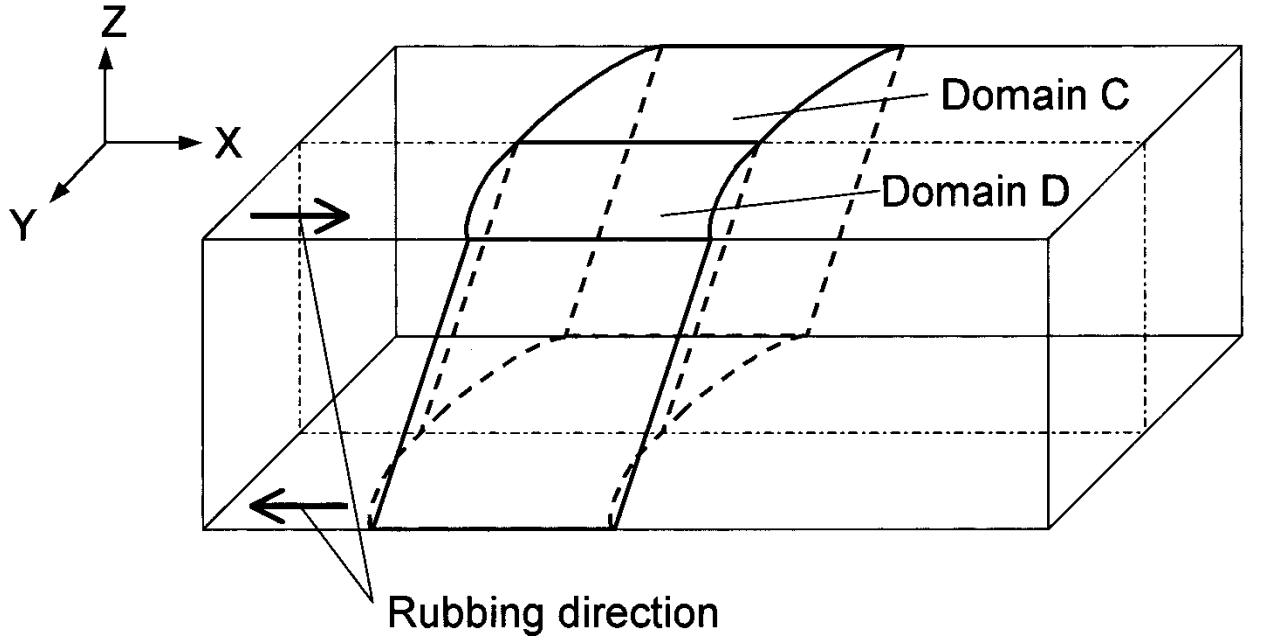

Figure 15. Schematic drawing of the proposed layer structure in sample 4, possessing the APD texture. The cell substrates lie in the XY-plane.

half-V FLC cells showed a stripe-shaped texture, it is proposed that the co-existence of the two structures forms the stripe-shaped patterns; that is, the tilted-bookshelf structure forms one kind of stripe and the near-bookshelf structure forms another kind of stripe.

The radius of the high-intensity area was nearly equal to the molecular tilt angle. That is, the layer tilt angle δ, the rotation angle α and the molecular tilt angle θ_{tilt} obeyed the relationship of equation (9). This result can explain how the half-V FLC exhibits a desirable black appearance in spite of the stripe-shaped texture, resulting in the substantially coincident extinction position of each domain.

By using a point-focused X-ray tube and optimizing the slit width, we succeeded in the two-axis measurement with a commercial X-ray system. The measurement provides information about the layer tilt angle and the layer rotation angle simultaneously and is a powerful tool for the analysis of smectic layer structure.

We thank T. Nonaka and H. Amakawa of Clariant Japan K. K. for supplying the half-V FLC materials and for fruitful discussion. We are also grateful to K. Saito of Philips Japan, Ltd for technical support regarding X-ray measurements.

References

[1] Takatoh, K., Yamaguchi, H., Hasegawa, R., Saishu, T., and Fukushima, R., 2000, *Polym. Adv. Technol.*, **11,** 413.

[2] Hasegawa, R., Fujiwara, H., Nagata, H., Hara, Y., Saishu, T., Fukushima, R., Akiyama, M., Okumura, H., and Takatoh, K., 2001, *J. SID*, **9,** 107.

[3] Hasegawa, R., Yamaguchi, H., Fukushima, R., and Takatoh, K., 2000, *Ferroelectrics*, **246,** 111.

[4] Asao, Y., Togano, T., Terada, M., Moriyama, T., Nakamura, S., and Iba, J., 1999, *Jpn. J. appl. Phys.*, **38,** 5977.

[5] Nonaka, T., Li, J., Ogawa, A., Hornung, B., Schmidt, W., Wingen, R., and Dübal, H., 1999, *Liq. Cryst.*, **26,** 1599.

[6] Ishiguro, H., and Kurita, T., 1996, *Tech. Rep. IEICE EID96-4*, **6,** 19 (in Japanese).

[7] Sueoka, K., Nakamura, H., and Taira, Y., 1997, in Proceedings of the International Display Research Conference, pp. 203–206.

[8] Patel, J. S., and Goodby, J. W., 1986, *J. appl. Phys.*, **59,** 2355.

[9] Hatano, T., Yamamoto, K., Takezoe, H., and Fukuda, A., 1986, *Jpn. J. appl. Phys.*, **25,** 1762.

[10] Myojin, K., Moritake, H., Ozaki, M., Yoshino, K., Tani, T., and Fujisawa, K., 1994, *Jpn. J. appl. Phys.*, **33,** 5491.

[11] Komitov, L., Lagerwall, S. T., Matuszczyk, M., and Stebler, B., 1996, *Ferroelectrics*, **189,** 199.

[12] Fünfschilling, J., and Schadt, M., 1998, *Ferroelectrics*, **213,** 195.

[13] Takada, K., Noma, T., Togano, T., Mukaide, T., and Iida, A., 2003, *Jpn. J. appl. Phys.*, **42,** 4431.

[14] Iida, A., Noma, T., and Miyata, H., 2001, *Jpn. J. appl. Phys.*, **40,** 1345.

[15] Takahashi, Y., Iida, A., Takanishi, Y., Ogasawara, T., Ishikawa, K., and Takezoe, H., 2001, *Jpn. J. appl. Phys.*, **40,** 3294.

[16] Takanishi, Y., Iida, A., Ishikawa, K., Takezoe, H., and Fukuda, A., 1999, *Jpn. J. appl. Phys.*, **38,** 4132.

[17] FINDON, A., GLEESON, H. F., and LYDON, J., 1998, *Liq. Cryst.*, **25,** 631.
[18] PARRY-JONES, L. A., BELDON, S. M., RODRIGUEZ-MARTIN, D., RICHARDSON, R. M., and ELSTON, S. J., 2002, *Liq. Cryst.*, **29,** 1001.
[19] WATSON, S. J., MATKIN, L. S., BAYLIS, L. J., BOWRING, N., and GLEESON, H. F., 2002, *Phys. Rev. E*, **65,** 031 705.
[20] RIEKER, T. P., CLARK, N. A., and SAFINYA, C. R., 1991, *Ferroelectrics*, **113,** 245.
[21] SHIN, S. T., BROCK, J. D., SUTTON, M., LITSTER, J. D., and KUMAR, S., 1998, *Phys. Rev. E*, **57,** R3711.
[22] SAFINYA, C. R., LIANG, K. S., VARADY, W. A., CLARK, N. A., and ANDERSSON, G., 1984, *Phys. Rev. Lett.*, **53,** 1172.
[23] CLARK, N. A., BELLINI, T., MALZBENDER, R. M., THOMAS, B. N., RAPPAPORT, A. G., MUZNY, C. D., SCHAEFER, D. W., and HRUBESH, L., 1993, *Phys. Rev. Lett.*, **71,** 3505.
[24] PARK, B., SEOMUN, S., NAKATA, M., TAKAHASHI, M., TAKANISHI, Y., ISHIKAWA, K., and TAKEZOE, H., 1999, *Jpn. J. appl. Phys.*, **38,** 1474.